Exploiting multipath fading with a mobile robot

Magnus Lindhé and Karl Henrik Johansson

The International Journal of Robotics Research 2013 32: 1363
DOI: 10.1177/0278364913486845

The International Journal of
Robotics Research
32(12) 1363–1380

DOI: 10.1177/0278364913486845
ijr.sagepub.com

Exploiting multipath fading with a mobile robot

Magnus Lindhé and Karl Henrik Johansson

Abstract

In indoor or urban applications, a moving robot with wireless communications will experience multipath fading. This causes rapid signal strength variations due to interfering reflections of the radio signal. By making short stops at positions with high signal-to-noise ratio (SNR), the robot can trade trajectory tracking accuracy for increased link quality. This represents a type of opportunistic communication-aware motion planning. We propose two novel strategies for improving the link capacity or throughput when either the robot has full knowledge of how the SNR varies along the trajectory, or when only the SNR distribution is known or can be estimated. In the latter case, this leads to an optimal stopping problem over a finite horizon. Both cases are analyzed for independent as well as correlated SNR samples, and a bounded maximum trajectory tracking error. We derive the resulting SNR distributions for the proposed strategies and use them to show how the expected capacity and throughput vary with the allowed tracking error. The results are confirmed by simulations and experiments. Experiments in six different locations validate the communication model and show that the proposed motion planning is robust to non-static fading and can yield throughput improvements of more than 100%.

Keywords

autonomous agents, networked robots, sensor networks, motion planning, multipath fading

1. Introduction

When controlling the motion of a mobile robot, some things to consider are robot dynamics, obstacle avoidance, navigation and energy efficiency. But in many applications, it is equally important to also account for maintaining communications, either with a base station or other robots. Reliable communications allow coordination between multiple robots, dissemination of sensor information, decentralized processing of data or intervention by an operator in the case of problems. There is growing awareness that communication considerations must be integrated from the beginning when designing robot controllers, to achieve good overall system performance. This paper presents one such approach to *communication-aware* motion planning.

We propose and analyze two strategies for communication-aware trajectory tracking for a robot moving through an environment which exhibits multipath fading. Multipath fading arises when wireless signals between a robot and a base station are reflected off objects surrounding the robot. The reflections can interfere constructively or destructively at the receiver antenna, which causes rapid variations in the signal strength when the robot moves just a fraction of a wavelength. In a static environment, the fading is a function only of the robot position. Thus, if the robot is allowed to deviate a small distance from the reference trajectory, it can improve the average link quality by making short stops at positions where the fading is favorable. This is illustrated in Figure 1. The first proposed strategy applies if the fading is known beforehand, such as if the robot has recently traversed the trajectory and can retrace it with high accuracy. It will mainly be used as a benchmark for the second strategy. The second strategy applies if only the statistics of the channel are known. The statistics can equivalently be estimated online, which is demonstrated in the experiments. Both strategies will be compared with the nominal strategy of driving at constant velocity.

The proposed strategies can be naturally integrated into existing architectures for motion planning. In practical robotic systems, it is common to separate the motion planning into layers (Varaiya, 2000). High-level tasks such as searching, coverage or transportation can be translated by a mission planner into ordered lists of waypoints for one

KTH Royal Institute of Technology, Stockholm, Sweden

Corresponding author:
Magnus Lindhé, KTH Royal Institute of Technology, Osquldas vaeg 10, 6tr, Stockholm 10044, Sweden.
Email: lindhe@ee.kth.se

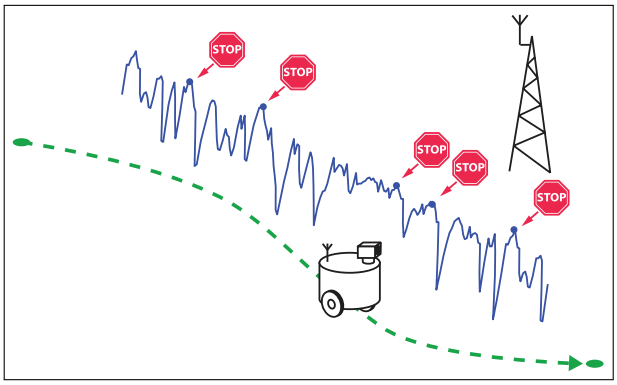

Fig. 1. A robot follows a reference trajectory while communicating with a base station, subject to multipath fading. By allowing the robot to deviate a bounded distance from the reference position, it can make short stops where the fading is favorable, thereby improving the average link quality.

or more robots. A path planner computes reference trajectories between the waypoints, avoiding obstacles and inter-robot collisions. On the lowest level, a motion controller uses continuous feedback from the sensors on each robot to track the reference trajectory with a given tolerance, compensating for disturbances and model errors. Our proposed strategies correspond to augmenting the motion controller so it also uses feedback from the radio when following the reference trajectory. The robot will stay on the reference path, which preserves obstacle avoidance, and the deviations are bounded, making it clear to higher layers what is sacrificed to gain communication quality. Our analysis clearly quantifies the tradeoff between link quality and tracking accuracy. First we briefly present some related work in communication-aware motion planning.

1.1. Related work

One way to categorize the literature on communication-aware motion planning is by the channel model used. There are several established models for radio signal propagation, each representing different tradeoffs between accuracy and simplicity of analysis. Below, we have roughly divided the related work into path loss models, shadowing and multipath fading. Note that some papers, particularly in the multipath fading category, also consider other propagation effects, but we have tried to isolate where the main contribution lies.

Path loss represents the decay of a radio signal due to the distance between transmitter and receiver. This is a deterministic effect that is well suited for analysis. A simple model is to assume perfect communication within a certain distance, and no connection outside it. This leads to a disc-shaped coverage region, well suited for multi-agent coordination under communication constraints, and has been applied to flocking (Zavlanos et al., 2009), coverage (Spanos and Murray, 2004), relaying (Tekdas et al., 2010) or rendezvous (Ji and Egerstedt, 2007). Instead of such a sharp threshold, one can let the packet loss rate or the magnitude of some additive noise increase with the distance. This allows joint optimization of communication and sensing objectives (Chung et al., 2006; Hsieh et al., 2008; Stachura and Frew, 2011) or motion planning for chains of routers (Stump et al., 2008). A related approach is to only assume that the signal strength is a sufficiently smooth function of the position, and then perform gradient estimation to try to improve the signal strength (Dixon and Frew, 2009). Models taking only path loss into account work well in space and open areas, but not in settings with obstacles.

Shadowing is the attenuation of radio signals due to obstacles. One way to model shadowing is to assume that robots are connected if and only if there is an unobstructed line of sight between them. There are examples of rendezvous (Ganguli et al., 2009), transportation (Esposito and Dunbar, 2006; Lindhé et al., 2011) and searching (Sweeney et al., 2004) problems, solved under these constraints. Connectivity can also be required only at certain time instances (Anisi et al., 2010; Hollinger and Singh, 2010). Line-of-sight models typically incorporate discontinuities that complicate analysis, and they are conservative since reflections or diffraction may make it possible to communicate even when there is no direct visibility. Another approach is to model the shadowing probabilistically, which helps to improve communication while solving sensing tasks (Ghaffarkhah and Mostofi, 2011).

Multipath fading is most pronounced in indoor or urban settings, where radio signals are scattered by objects. Since the fading has a complex dependence on the layout of the environment, it is usually treated as a stochastic effect. Even small movements of an antenna will change the fading, which can be exploited to improve the signal strength for a stationary (Lindhé et al., 2007; Smith et al., 2009) or mobile (Lindhé and Johansson, 2009) sensor node. If nodes are connected in a network, such small movements will change the capacities of the links, which may be used for load balancing (Puccinelli et al., 2007) or for improving the network throughput (Vieira et al., 2011). Estimating the spatial correlation of the fading can also give important information. Mobile sensors can adapt the step size of their movement so as to faster escape from deep fades (Mostofi, 2009). The stochastic model of multipath fading makes planning difficult and the effect is less significant if there is a strong direct component in the signal, compared to the reflections.

1.2. Contributions

This paper contains four major contributions. The first is a novel problem formulation for exploiting multipath fading, which considers both the case of full channel knowledge and the case when only the channel statistics are known. We impose hard bounds on the tracking error, making it clear to a system designer how much tracking accuracy is sacrificed for improved link quality. The system uses feedback from the instantaneous signal-to-noise ratio (SNR) to

control when to stop the robot. The second contribution is to consider a broad communication model, assuming Nakagami fading (which includes Rayleigh fading as a special case) and allowing correlated samples of the signal strength, which makes the analysis more involved. The third contribution is that we provide analytical expressions, verified by simulations, for the resulting distribution of the SNR, which can be used to compute the expectation of various parameters of the channel. The final contribution is validation measurements for the communication model in several locations, as well as experimental comparison of two of the proposed strategies. Results for the latter show significant improvements in average throughput compared with the nominal case. We have considered motion planning under multipath fading in earlier preliminary studies, but without bounds on the tracking error, only assuming known channel statistics and using time-triggered or state-triggered stopping (Lindhé and Johansson, 2009).

1.3. Outline

In the following section, we present models of the robot motion and the wireless channel. We then formally define the problem, under five different assumptions on the available channel information. In Section 3, we propose a motion strategy to maximize the link quality for each of the five cases. In Section 4, we derive the resulting SNR distribution of each strategy, which can be used to compute the expectation of various quantities of interest. To illustrate this, Section 5 shows how the expected link capacity and throughput vary with the allowed deviation from the reference trajectory. We also compare the analytical results with simulations. Then Section 6 presents measurements to validate the communication model, as well as experimental results on the comparison of two of the strategies. We end by conclusions and some ideas on possible future research.

2. Preliminaries

In this section, we present models of the robot motion and the communication channel. We then continue by formulating the problem.

2.1. Robot model

We assume that a path planner as mentioned above provides an obstacle-free reference trajectory $q_{\text{ref}}(t) : [0, T] \to \mathbb{R}^2$ with constant speed and some final time T. Let $x(t)$, $x_{\text{ref}}(t) \in \mathbb{R}$ be the position along the path, $\bigcup_{t\in[0,T]} q_{\text{ref}}(t)$, of the robot and the reference position, respectively. In the following, we study the reference tracking error, $\Delta(t) \triangleq x(t) - x_{\text{ref}}(t)$. It has the following dynamics

$$\dot{\Delta}(t) = v(t) - v_{\text{ref}}, \tag{1}$$

where $v_{\text{ref}} \triangleq \dot{x}_{\text{ref}}(t)$ is assumed to be constant and $v(t) \triangleq \dot{x}(t)$. The path is assumed smooth enough for the robot to be able to follow it at any velocity $v(t) \in [0, v_{\max}]$. We restrict the velocity to be non-negative to avoid wasting energy by covering the same path multiple times. This kinematic model is reasonable for ground robots with high gear ratio motors, which can change their velocities almost instantaneously. The assumption on constant reference velocity simplifies the discussion of the results in the paper. As becomes clear below, it is not essential for the proposed motion planning strategies.

2.2. Communication model

We assume that the robot is communicating with a fixed base station while moving in an environment that exhibits multipath fading. Owing to the complex dependence on the environment geometry, the fading is usually modeled as a stochastic process (Molisch, 2005). We use the standard model of Nakagami fading, which shows good agreement with measurements, both in urban (Sarkar et al., 2003; Rubio et al., 2007) and indoor (Sheikh et al., 1993; Babich and Lombardi, 2000) environments. Under Nakagami fading, the SNR, γ, is gamma distributed with probability density function (PDF)

$$f_\gamma^N(\gamma) = \frac{m}{\Omega\Gamma(m)} \left(\frac{m\gamma}{\Omega}\right)^{m-1} \exp\left(\frac{-m\gamma}{\Omega}\right). \tag{2}$$

Here, $\Omega \triangleq \mathrm{E}[\gamma]$ is the mean SNR, $\Gamma(\cdot)$ is the Gamma function and m is the Nakagami parameter

$$m \triangleq \frac{\Omega^2}{\mathrm{E}[(\gamma - \Omega)^2]}, \tag{3}$$

which describes the severity of the fading. The case $m = 1$ is Rayleigh fading, and for $m \to \infty$, the distribution becomes an impulse, corresponding to no fading. The cumulative distribution function (CDF) for γ can be obtained by integration of (2) as

$$F_\gamma^N(z) \triangleq P(\gamma < z) = \frac{\gamma_{\text{inc}}(m, \frac{mz}{\Omega})}{\Gamma(m)}, \tag{4}$$

where $\gamma_{\text{inc}}(s, w) = \int_0^w e^{-t} t^{s-1}\, \mathrm{d}t$ is the incomplete gamma function. We consider transceivers with narrow bandwidth, so the fading is assumed flat. This means that all frequencies of the signal are affected equally, so we only get attenuation, not distortion. Further, the transceivers are assumed to move slowly enough for the fading to be slow, i.e. the channel is constant over the duration of one transmitted bit.

It is assumed that the parameters Ω and m can change along the path, but much slower than the variations due to multipath fading. We further assume *static fading*, meaning that the fading is only a function of the position of the robot, so if it stands still, the SNR is constant. We therefore denote the SNR as $\gamma(x)$. This is the case if the robot is the only moving object in the environment, which applies to scenarios such as nighttime surveillance, rescue missions inside collapsed buildings and bomb disposal. Static fading

is well described in the literature (Puccinelli and Haenggi, 2006; Smith et al., 2009), and we will validate this assumption experimentally and test what happens if it is violated. We also note that for given positions of the base station and the robot, the channel is symmetric, so the fading causes the same attenuation of the signal in both directions.

The correlation of the SNR at two points along the path is, in general, a function of the distance between them and their orientation relative to any dominant line-of-sight component of the signal. For simplicity, we assume uniform scattering, so signal components from all directions have equal strength, and straight paths, so the distance between two points is equal to the difference in position along the path. (If there is a dominant component, the correlation depends on its angle relative to the path (Stüber, 1996, Sec. 2.1.3) and for a given path with curvature it is straightforward to compute the actual distance between two positions with given x-coordinates.) In this case, the correlation coefficient of $\gamma(x)$ and $\gamma(x+\delta)$ is

$$\begin{aligned}\rho &= \frac{\mathrm{E}[(\gamma(x)-\Omega)(\gamma(x+\delta)-\Omega)]}{\sqrt{\mathrm{E}[(\gamma(x)-\Omega)^2]\,\mathrm{E}[(\gamma(x+\delta)-\Omega)^2]}} \\ &= J_0^2(2\pi\delta/\lambda), \end{aligned} \tag{5}$$

where λ is the wavelength and J_0 is the zeroth-order Bessel function of the first kind (Molisch, 2005, Equation (13.4)). The correlation has a zero at $\delta = 0.38\lambda$ and two samples are often considered independent if the inter-sample distance is greater than $\lambda/2$ (Jakes, 1974). In the analysis, we will use this assumption. In the experiments in Section 6, we will consider samples to be independent already at a separation of $\lambda/4$, when the amplitude correlation coefficient has decreased below 0.5. This is another common assumption which allows denser sampling without the increased complexity of considering correlation (Molisch, 2005).

There are several possible metrics for the quality of the wireless link. In this paper, we consider two types of utility functions $U(\gamma)$. The first is the maximum channel capacity $U_{\mathrm{C}}(\gamma) \triangleq B\log_2(1+\gamma)$, where B is the bandwidth of the channel. The second is the throughput $U_{\mathrm{T}}(\gamma) = R_0(1-P_b(\gamma))^{8M}$, where $P_b(\gamma)$ is the bit error probability, M is the number of bytes in a packet and R_0 is the packet transmission rate. The throughput describes the rate of packets delivered to the receiver and will be used as the quality metric in the experiments. Note that it would be straightforward to apply the same analysis to other utilities, as long as $U(\gamma)$ is strictly increasing with γ so the inverse U^{-1} exists. The expectation of a given utility depends on the SNR distribution f_γ as

$$E[U(\gamma)] = \int_0^\infty U(\gamma) f_\gamma(\gamma)\,\mathrm{d}\gamma. \tag{6}$$

By performing communication-aware motion, we can affect the resulting SNR distribution f_γ so that it yields higher expected utility than the nominal distribution f_γ^N. In the following, we will call these the *resulting* and *nominal* SNR distributions, respectively.

Table 1. Available channel information.

A priori information	Sparse sampling ($\delta \geq \lambda/2$)	Dense sampling ($\delta < \lambda/2$)
None	Case 0	
Known distribution of $\gamma(x_i)$	Case 1A	Case 1B
Full knowledge of $\gamma(x_i)$	Case 2A	Case 2B

The robot is assumed to be able to measure the link SNR, either by comparing the received signal strength (RSS) of received packets with the general noise level, or by getting reports back from the base station. We will assume that it can sample the SNR at equidistant positions,

$$x_i \triangleq \delta i, \quad i = 0, 1, \ldots, \left\lfloor \frac{T v_{\mathrm{ref}}}{\delta} \right\rfloor,$$

along the path, where δ is the distance between samples. We also define the notation $\gamma_i \triangleq \gamma(x_i)$. In the following, we will distinguish between *sparse sampling*, when $\delta \geq \lambda/2$ so the SNR samples can be regarded as independent, and *dense sampling*, when $\delta < \lambda/2$ so the samples are considered correlated.

2.3. Problem formulation

In an environment with multipath fading as described above, the average utility of the wireless channel between the robot and the base station could be increased by giving the robot freedom to deviate some from the reference position, to allow it to spend more time at positions where the utility is high. The robot can only get information about the SNR at the sampling points, x_i, so to maximize the time available to spend at points with high SNR, we assume that it always moves at $v_{\max}$ between sampling points. The problem is then how long to stop at each sampling point or, equivalently, to control the velocity $v(t)$:

We consider a robot with dynamics (1), moving along a path in an environment with static Nakagami fading, where the SNR is distributed according to the nominal distribution (2), with spatial correlation (5). The position $x(t)$ and tracking error $\Delta(t)$ are known, and the robot has access to channel information as specified in Table 1. Find a *stopping strategy*, i.e. a rule that determines how long to stop at the current sampling point, that yields high expected channel utility (6) while maintaining a bounded tracking error $|\Delta(t)| \leq \Delta_{\max}\ \forall\, t \in [0, T]$. We assume that $\Delta_{\max} > \delta/2$, so the robot can always reach at least one sampling position.

We will study five different cases of available channel information. They differ in the amount of *a priori* information available and the SNR sampling density, as defined in Table 1.

Having no *a priori* information (case 0) is the nominal case, which we will use as a reference. In cases 1A and 1B, the nominal joint distribution of all SNR samples is assumed known. In practice, this could be predicted from

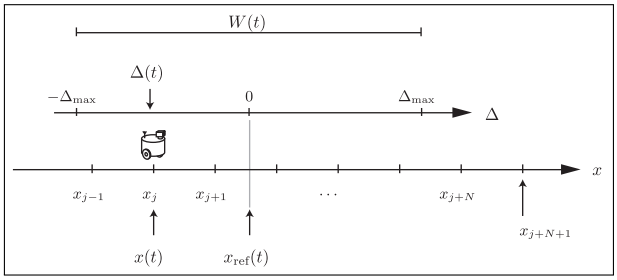

Fig. 2. Illustration of the tracking window, $W(t)$, i.e. the interval where $|\Delta(t)| \leq \Delta_{\max}$ so reference tracking is maintained. From the current sample position x_j, the robot can reach $x_{j+1}, \ldots, x_{j+N}$ by driving at $v_{\max}$, without stopping. It cannot reach x_{j+N+1} without stopping first, since then it would go outside of $W(t)$.

a map or estimated online, based on previous SNR samples. Finally, if the robot has already traversed the path, it could store the full SNR as function of position, which corresponds to cases 2A or 2B. Note that this also requires accurate navigation, as even small deviations from the previous path will reduce the correlation between the current SNR and old measurements. For each case, we will derive the resulting SNR distribution f_γ^j, $j \in \{0, 1\text{A}, 1\text{B}, 2\text{A}, 2\text{B}\}$. This distribution can be used to compute the expectation of any utility.

3. Stopping strategies

In this section, we describe receding horizon stopping strategies for each case above. We first derive the decision horizon for the robot at each decision instance. We define the *tracking window*, $W(t) \in \mathbb{R}$, as

$$W(t) \triangleq \{x : |x - x_{\text{ref}}(t)| \leq \Delta_{\max}\},$$

i.e. the x-interval where the tracking constraint is satisfied. Note that the window moves along the path at velocity v_{ref}. As stated above, the robot always drives at $v_{\max}$ between the sampling points, so it only needs to make stop-or-go decisions at sampling points. We denote the current sampling point as x_j, where at time t, $j = x(t)/\delta$. From x_j, if the robot drives at $v_{\max}$ without stopping, it can reach the positions $x_{j+1}, \ldots, x_{j+N}$, where

$$N = \left\lfloor \frac{\Delta_{\max} - \Delta(t)}{\delta(1 - v_{\text{ref}}/v_{\max})} \right\rfloor. \tag{7}$$

This is illustrated in Figure 2. It cannot reach x_{j+N+1} without stopping, since then it would violate the tracking constraint. Thus, the robot must stop at one of the $N+1$ positions $x_j, \ldots, x_{j+N}$ for some time. Then the sample x_{j+N+1} becomes reachable, and a new decision should be made.

The above discussion shows that when making a stop-or-go decision, the stopping strategy only needs to consider a horizon of N future SNR samples. Note that the driving time between samples does not need to be considered, since the robot needs to traverse the whole path in a constant time T, regardless of the stopping strategy. It will thus spend the time $Tv_{\text{ref}}/v_{\max}$ driving, passing each part of the trajectory once. Hence, the utility during this time is independent of the stopping strategy. With this background, we now present stopping strategies for each case of channel information.

3.1. No channel information (case 0)

Without knowing the channel statistics, the robot cannot determine whether a given SNR sample is worth stopping at or not. Thus, we propose a stopping strategy that maintains a low tracking error, Δ:

Uninformed stopping strategy: Stand still at x_j until $\Delta(t) < -\delta/2$, then continue to x_{j+1}.

This strategy means that the robot stays close to the center of the tracking window at all times. Note that the robot could still sample the SNR at all stops and quickly have enough information for estimating f_γ^N. Then it could switch to the partially informed stopping strategy, described below, if it needs to improve the channel utility.

3.2. Known nominal SNR distribution

Knowing the nominal SNR distribution, the robot can compare the current utility with what can be expected further ahead. The decision to stop at a position where the utility is high or continue exploring forward can then be formulated as an optimal stopping problem (Chow, 1971). We now derive the optimal stopping rules for this problem in the cases of sparse and dense sampling, respectively, and then summarize them in a proposed *partially informed* strategy.

After sampling γ_j inside $W(t)$, the robot can either stop there, which yields the utility $U(\gamma_j)$, or move forward to the next sample. If the robot rejects γ_j, there are N samples left to choose from, so if it reaches γ_{j+N}, it must stop. This is an instance of Moser's problem of optimal stopping, which can be solved by induction (Moser, 1956). The result is a threshold function $\bar{\gamma}(N)$ such that the robot should stop at x_j if and only if $\gamma_j > \bar{\gamma}(N)$. Note that the threshold function will also depend on the sampling density, δ. Below, we derive the threshold functions for the case of sparse and dense sampling, respectively.

3.2.1. Sparse sampling (case 1A) Define the maximal expected utility, when starting from sample γ_j, as

$$V_j(\gamma_j) \triangleq \max\{U(\gamma_j), \mathrm{E}[V_{j+1}(\gamma_{j+1})]\}.$$

If the robot arrives at x_{j+N}, it has to stop, so $V_{j+N}(\gamma_{j+N}) = U(\gamma_{j+N})$. We define $A_{j+k} \triangleq \mathrm{E}[V_{j+k}(\gamma_{j+k})]$, where

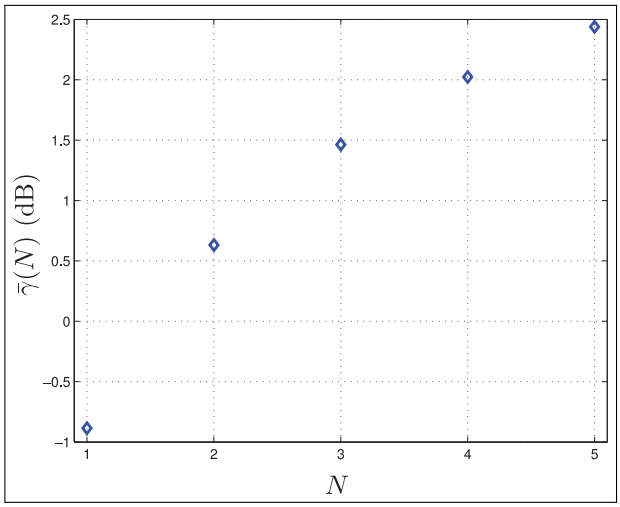

Fig. 3. Stop thresholds for the partially informed stopping strategy, maximizing the capacity and assuming independent SNR samples (case 1A). If the robot has N future samples to select from, it should stop at x_j if $\gamma_j > \bar{\gamma}(N)$. Note that $\bar{\gamma}(0)|_{\text{dB}} = -\infty$.

$k \in \{1, \ldots, N\}$ and $A_{j+N+1} \triangleq 0$. We compute A_{j+k} through the induction

$$A_{j+k} = \mathrm{E}[\max\{U(\gamma_{j+k}), A_{j+k+1}\}] = \int_0^{U^{-1}(A_{j+k+1})} A_{j+k+1} f_\gamma^N(\gamma)\, \mathrm{d}\gamma + \int_{U^{-1}(A_{j+k+1})}^{\infty} U(\gamma) f_\gamma^N(\gamma)\, \mathrm{d}\gamma.$$

The robot should stop if the current utility is higher than the maximal expected utility ahead, so the stop threshold for γ_j is $\bar{\gamma}(N) = U^{-1}(A_{j+1})$. We remind the reader that, through the induction above, A_{j+1} depends on N, which depends on $\Delta(t)$. As an example, if $\Delta_{\max} = \lambda$, $N \leq 5$, and the thresholds $\bar{\gamma}(N)$ for $N = 1, \ldots, 5$ are depicted in Figure 3. In the figure, we have assumed $U = U_{\mathrm{C}}$, $m = 1$ and $\Omega = 0$ dB.

3.2.2. Dense sampling (case 1B) The correlation coefficient for any two samples γ_i and γ_j can be computed by (5), with separation $\delta|i - j|$. We define the maximal expected utility that can be found after sampling until γ_j as

$$\tilde{V}_j(\gamma_1, \ldots, \gamma_j) \triangleq \max\{U(\gamma_j), \mathrm{E}[\tilde{V}_{j+1}(\gamma_1, \ldots, \gamma_{j+1}) \mid \gamma_1, \ldots, \gamma_j]\}.$$

Of course, $\tilde{V}_{j+N}(\gamma_1, \ldots, \gamma_{j+N}) = U(\gamma_{j+N})$. We define

$$\tilde{A}_{j+k}(\gamma_1, \ldots, \gamma_{j+k-1}) \triangleq \mathrm{E}[\tilde{V}_{j+k}(\gamma_1, \ldots, \gamma_{j+k}) \mid \gamma_1, \ldots, \gamma_{j+k-1}].$$

As above, we can let $\tilde{A}_{j+N+1}(\gamma_1, \ldots, \gamma_N) = 0$ and inductively compute

$$\tilde{A}_{j+k}(\gamma_1, \ldots, \gamma_{j+k-1}) = \int_0^{\infty} \tilde{V}_{j+k}(\gamma_1, \ldots, \gamma_{j+k}) f^N_{\gamma_{j+k}|\gamma_1, \ldots, \gamma_{j+k-1}} (\gamma_{j+k}|\gamma_1, \ldots, \gamma_{j+k-1})\, \mathrm{d}\gamma_{j+k},$$

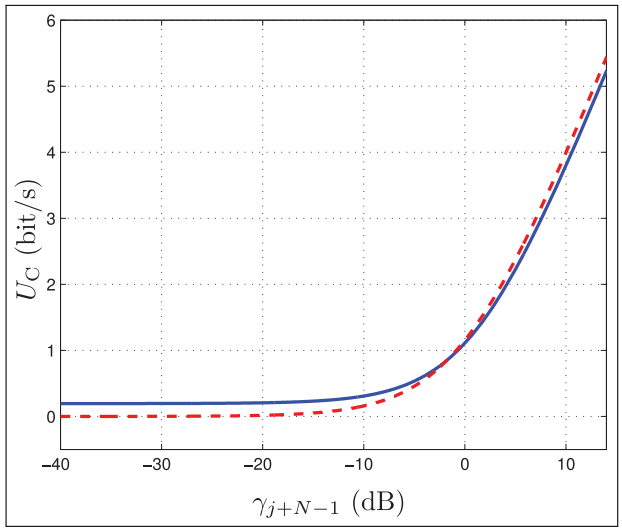

Fig. 4. The first step in the induction to find stop thresholds for case 1B. The expected channel capacity at the last sample, $\tilde{A}_{j+N}(\gamma_{j+N-1})$, is plotted as a solid line. If it is less than the capacity at the current sample, $U_{\mathrm{C}}(\gamma_{j+N-1})$ (dashed line), the robot should stop. In this case, with $\rho = 0.87$, $m = 1$ and $\Omega = 0$ dB, the threshold is -1.7 dB, where the curves intersect.

where $f^N_{\gamma_{j+k}|\gamma_1, \ldots, \gamma_{j+k-1}}$ can be computed from the multivariate Nakagami PDF $f^N_{\gamma_1, \ldots, \gamma_{j+k}}$ (Aalo, 1995). Finding $\tilde{A}_j(\gamma_1, \ldots, \gamma_{j-1})$ requires computing an N-dimensional integral, which is computationally intractable as N grows.

To make the problem tractable, we propose a Markov assumption: since the correlation decays quickly with distance, we only consider the correlation between adjacent samples. This yields the simplified induction

$$\tilde{A}_{j+k}(\gamma_1, \ldots, \gamma_{j+k-1}) \approx \tilde{A}_{j+k}(\gamma_{j+k-1}) = \int_0^{\infty} \tilde{V}_{j+k}(\gamma_{j+k-1}, \gamma_{j+k}) f^N_{\gamma_{j+k}|\gamma_{j+k-1}}(\gamma_{j+k}|\gamma_{j+k-1})\, \mathrm{d}\gamma_{j+k},$$

which can be computed as a two-dimensional integral. To illustrate the first step of the induction, Figure 4 shows $\tilde{A}_{j+N}(\gamma_{j+N-1})$, for $U = U_{\mathrm{C}}$, $m = 1$ and $\Omega = 0$ dB. We assume a sample spacing of $\delta = \lambda/12$, which gives a pairwise correlation coefficient of $\rho = 0.87$. We have assumed $B = 1.15$ Hz so the expected capacity for $f_\gamma^N(\gamma)$ is 1 bit/s. The solid line depicts $\tilde{A}_{j+N}(\gamma_{j+N-1}) = \mathrm{E}[\tilde{V}_{j+N}(\gamma_{j+N})|\gamma_{j+N-1}]$. After sampling γ_{j+N-1}, the robot will stop if $U(\gamma_{j+N-1})$ (dashed line) is higher than $\tilde{A}_{j+N}(\gamma_{j+N-1})$, or equivalently if $\gamma_{j+N-1} > U^{-1}(\tilde{A}_{j+N}(\gamma_{j+N-1}))$. Otherwise, it moves on to x_{j+N}. The threshold for stopping at x_j is thus the intersection of the graphs, i.e. $\bar{\gamma}(N) = \gamma : U(\gamma) = \tilde{A}_{j+1}(\gamma)$. The graphs are flat at the intersection, but we have not experienced any accuracy problems in our simulations. As an example, if $\Delta_{\max} = \lambda$, $N \leq 30$ in this case, and the thresholds for $N = 1, \ldots, 30$ and $U = U_{\mathrm{C}}$ are shown in Figure 5.

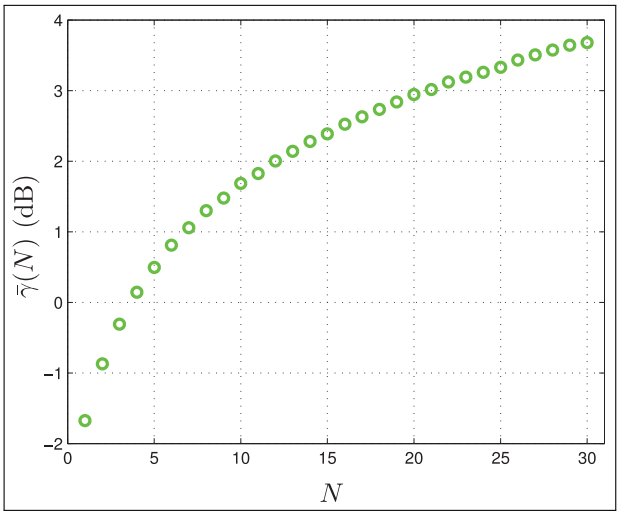

Fig. 5. Stop thresholds for the partially informed stopping strategy, maximizing the capacity and assuming correlated SNR samples (case 1B). If the robot has N future samples to select from, it should stop at x_i if $\gamma_i > \bar{\gamma}(N)$. Note that $\bar{\gamma}(0)|_{\text{dB}} = -\infty$.

To summarize this section, we have now computed the optimal stopping thresholds for the following proposed strategy for cases 1A and 1B.

Partially informed stopping strategy: Stand still at x_j while $\Delta(t) > -\Delta_{\max}$ and $\gamma_j > \bar{\gamma}(N)$, where N is computed from $\Delta(t)$ as in (7) and $\bar{\gamma}(N)$ is computed by induction as shown above, for either independent or correlated samples. Otherwise, continue to x_{j+1}.

Note that the robot will never violate the tracking constraint by exceeding $\Delta_{\max}$, since the stop threshold for $N = 0$ is $\bar{\gamma}(0) = 0$. We now continue to the cases when the robot has full information of the SNR as function of the position.

3.3. Full channel knowledge (cases 2A and 2B)

If the robot knows the SNR along the whole path, we can expect higher resulting channel utility than when only the distribution is known. With full channel knowledge, the optimal strategy does not depend on the choice of utility:

Fully informed stopping strategy: Stand still at x_j while $\Delta(t) > -\Delta_{\max}$ and $\gamma_j = \max\{\gamma_j, \ldots, \gamma_{j+N}\}$, where N is computed from $\Delta(t)$ as in (7). Otherwise, continue to x_{j+1}.

As above, the robot will never violate the tracking constraint by exceeding $\Delta_{\max}$, since if $N = 0$, the second stopping condition is vacuously satisfied. We now continue to analyzing the resulting performance of each stopping strategy.

4. Performance analysis

In this section, we derive the resulting SNR distributions for each case, under the proposed stopping strategies above. The distributions can be used to compute the expectation with respect to various utilities. We will give some examples of this in Section 5.

4.1. No channel information (case 0)

When the motion is independent of the SNR, the resulting SNR has the nominal distribution:

$$f_\gamma^0(\gamma) = f_\gamma^N(\gamma).$$

We will use this later, assuming that whenever the robot drives at constant velocity, it experiences the nominal SNR distribution f_γ^N.

4.2. Known nominal SNR distribution

To derive the resulting SNR distribution when the nominal distribution is known, we first compute the distribution of the value of N when the robot arrives at a sample. Using this, we can derive the CDF of the SNR experienced while standing still. Finally, we add the influence of the SNR distribution experienced when driving, as derived above.

To begin, we note that when standing still, the decision instances for the robot occur when $\Delta_{\max} - \Delta(t)$ is an even multiple of $\delta(1 - v_{\text{ref}}/v_{\max})$, i.e. with constant intervals. If the robot decides to drive, $\Delta(t)$ increases by

$$\frac{\delta}{v_{\max}}(v_{\max} - v_{\text{ref}}) = \delta\left(1 - \frac{v_{\text{ref}}}{v_{\max}}\right).$$

Thus, the robot always stands still for an equal amount of time between decision instances. Hence, to find the resulting SNR distribution when standing still, we can find the distribution of the SNR for each stop interval, as they have equal duration. The horizon length N, i.e. the number of samples ahead that the robot can choose from, will vary over time as it is a function of $\Delta(t)$. The discussion above implies that N increases by one when the robot stands still for one stop interval, and decreases by one if the robot drives ahead to the next sampling position. We will use this in the analysis. We define N_j as the value of N when the robot arrives at the sample position x_j and stop_j as the event that, at a decision instance, the robot chooses to stand still at x_j. We further define the highest possible value of N as

$$N_{\max} \triangleq \left\lfloor \frac{2\Delta_{\max}}{\delta(1 - v_{\text{ref}}/v_{\max})} \right\rfloor.$$

To model the fact that the robot is forced to drive when $\Delta(t) \leq -\Delta_{\max}$, we can assume that $\bar{\gamma}(N_{\max}) = \infty$. The cases of sparse and dense sampling are now treated separately.

4.2.1. Sparse sampling (case 1A) The robot will leave x_{j-1} and go to x_j when $\gamma_{j-1} \leq \bar{\gamma}(n)$ for some $n \leq N_{\max}$. Then $N_j = n - 1$. And since N decreases only when the robot advances to the next sample position, the SNR at a sample

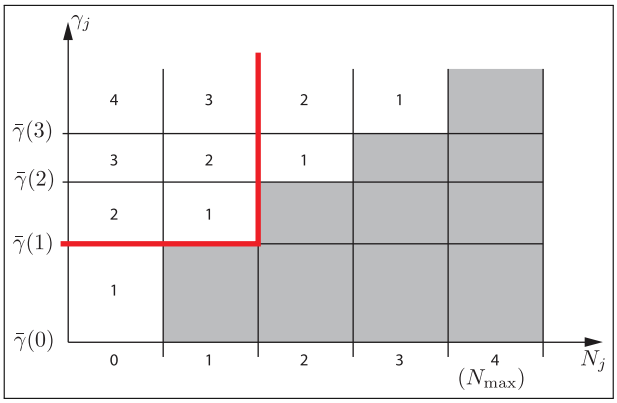

Fig. 6. The time that the robot stands still at a sample position x_j is determined by N_j, the value of N when it arrives, and γ_j. Shaded grids correspond to the robot not stopping, and white grids contain the number of time slots that the robot stands still for those values of N_j and γ_j. This illustrates the case $N_{\max} = 4$ and the thick line indicates the half-open set where $N_j \leq 1$ and $\gamma_j > \bar{\gamma}(1)$.

position k steps back cannot have exceeded $\bar{\gamma}(N_j + k)$. For some integer $n \in \{0, \ldots, N_{\max}\}$, the event that $N_j \leq n$ is therefore equivalent to

$$\gamma_{j-k} \leq \bar{\gamma}(n+k) \;\forall\, k \in \{1, \ldots, k_{\max}\}, \tag{8}$$

where $k_{\max} \triangleq N_{\max} - n - 1$. Note that these are all independent events. Condition (8) is necessary since if there is any $k \in \{1, \ldots, k_{\max}\}$ such that $\gamma_{j-k} > \bar{\gamma}(n+k)$, then $N_{j-k+1} > n + k - 1$, which implies that $N_j > n$. It is also sufficient, since it implies that $N_{j-k} \leq n + k$. This shows that the probability that $N_j \leq n$ is

$$P(N_j \leq n) = \prod_{k=1}^{k_{\max}} P(\gamma_{j-k} < \bar{\gamma}(n+k)). \tag{9}$$

We now have a distribution for N_j, i.e., the value of N as the robot arrives at x_j. Figure 6 shows how N_j and γ_j determine the number of stop intervals that the robot spends at x_j.

The CDF of γ_j, given that the robot decides to stand still, can thus be computed as follows:

$$P(\gamma_j < z|\text{stop}_j) = \frac{\sum_{n=0}^{N_{\max}-1} P(N_j \leq n) P(\bar{\gamma}(n) < \gamma_j < z)}{\sum_{n=0}^{N_{\max}-1} P(N_j \leq n) P(\gamma_j > \bar{\gamma}(n))},$$

Here, each term is weighted by $k + 1$, which is the number of stop intervals corresponding to each combination of N_j and γ_j. The double sums can be simplified to a single sum, computed over half-open sets as the one indicated by the thick line in Figure 6. This yields

$$P(\gamma_j < z|\text{stop}_j) = \frac{\sum_{n=0}^{N_{\max}-1} \sum_{k=0}^{k_{\max}} (k+1) P(N_j = n) P(\bar{\gamma}(n+k) < \gamma_j < \bar{\gamma}(n+k+1) \wedge \gamma_j < z)}{\sum_{n=0}^{N_{\max}-1} \sum_{k=0}^{k_{\max}} (k+1) P(N_j = n) P(\bar{\gamma}(n+k) < \gamma_j < \bar{\gamma}(n+k+1))}.$$

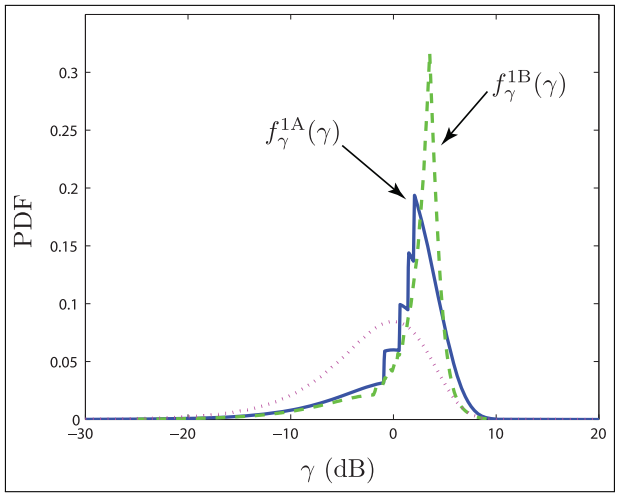

Fig. 7. Resulting SNR distributions for the cases of *a priori* knowledge of the channel statistics and a maximal tracking error of $\Delta_{\max} = \lambda$. The PDF $f_\gamma^{1A}(\gamma)$ (solid line) assumes 5 samples taken $\lambda/2$ $f_\gamma^{1B}(\gamma)$ (dashed line) assumes 30 correlated samples taken $\lambda/12$ apart. The Nakagami distribution (dotted line), is included for comparison. It corresponds to driving at constant velocity, as in case 0. By communication-aware motion planning, the centers of mass of $f_\gamma^{1A}(\gamma)$ and $f_\gamma^{1B}(\gamma)$ are displaced towards higher SNR values than the nominal PDF of case 0.

which can be computed using the CDF (4), (9) and

$$P(\bar{\gamma}(n) < \gamma_j < z) = \max\{0, P(\gamma_j < z) - P(\gamma_j < \bar{\gamma}(n))\}.$$

Hence, the PDF for γ when standing still at some sample position x_j can be computed as

$$f_{\text{stop}}^{1A}(z) = \frac{\mathrm{d}}{\mathrm{d}z} P(\gamma_j < z|\text{stop}_j). \tag{10}$$

To find the overall resulting SNR distribution for case 1A, we recall that the fraction $v_{\text{ref}}/v_{\max}$ of the time is spent driving, when the robot experiences the nominal SNR distribution f_γ^N. The rest of the time is spent standing still at an SNR sample, whose distribution is given by (10). Over the whole trajectory, the resulting SNR experienced by the robot is thus distributed as

$$f_\gamma^{1A}(\gamma) = \left(1 - \frac{v_{\text{ref}}}{v_{\max}}\right) f_{\text{stop}}^{1A}(\gamma) + \frac{v_{\text{ref}}}{v_{\max}} f_\gamma^N(\gamma), \tag{11}$$

which is illustrated by the solid line in Figure 7. The figure assumes $\delta = \lambda/2$, $\Delta_{\max} = \lambda$ and $v_{\text{ref}}/v_{\max} = 0.2$.

We now move on to the case of dense sampling, where the samples can no longer be assumed independent.

4.2.2. Dense sampling (case 1B) The analysis is similar to case 1A, but using conditional probabilities. As above,

$$P(N \leq n|\gamma_j) = P(\gamma_{j-1} < \bar{\gamma}(n+1)\,|\gamma_j) \times \prod_{k=2}^{k_{\max}} P(\gamma_{j-k} < \bar{\gamma}(n+k)\,|\gamma_{j-k+1} < \bar{\gamma}(n+k-1))\,.$$

After simplification, the CDF of γ_j, given that the robot is standing still at x_j is

$$P(\gamma_j < z|\text{stop}_j) = \frac{\sum_{n=0}^{N_{\max}-1} P(N_j \leq n|\bar{\gamma}(n) < \gamma_j < z)\,P(\bar{\gamma}(n) < \gamma_j < z)}{\sum_{n=0}^{N_{\max}-1} P(N_j \leq n|\gamma_j > \bar{\gamma}(n))\,P(\gamma_j > \bar{\gamma}(n))}.$$

The conditional probabilities above can be computed using the bivariate Nakagami PDF $f^N_{\gamma_1,\gamma_2}(\gamma_1,\gamma_2)$ (Simon and Alouini, 1998):

$$P(\gamma_1 < z_1|z_2 < \gamma_2 < z_2') = \frac{\int_0^{z_1}\int_{z_2}^{z_2'} f^N_{\gamma_1,\gamma_2}(s,t)\;\mathrm{d}t\,\mathrm{d}s}{\int_0^{\infty}\int_{z_2}^{z_2'} f^N_{\gamma_1,\gamma_2}(s,t)\;\mathrm{d}t\,\mathrm{d}s}. \quad (12)$$

As in case 1A, the robot will spend a fraction $v_{\text{ref}}/v_{\max}$ of the time driving, and the rest of the time standing still. The resulting overall PDF for the SNR is then

$$f^{1\text{B}}_{\gamma}(\gamma) = \left(1 - \frac{v_{\text{ref}}}{v_{\max}}\right)\frac{\mathrm{d}}{\mathrm{d}z}P(\gamma_j < z|\text{stop}_j) + \frac{v_{\text{ref}}}{v_{\max}}f^N_{\gamma}(\gamma), \quad (13)$$

which is plotted as a dashed line in Figure 7. The figure assumes $\delta = \lambda/12$, $\Delta_{\max} = \lambda$ and $v_{\text{ref}}/v_{\max} = 0.2$.

4.3. Full channel knowledge

Under the fully informed stopping strategy, if the robot chooses to stop at a sample γ_j, this is the best out of $N_{\max}$ samples. Selecting the best out of $N_{\max}$ SNR samples taken with a mobile robot is equivalent to selection combining diversity, where a receiver selects the best out of $N_{\max}$ antennas. For antennas separated enough so they can be considered independent, the analysis is straightforward, as we will see below. For correlated antennas, there are exact expressions for the joint PDF, but in practice they are computationally intractable for $N_{\max} > 4$ (Zhang and Lu, 2002). Alternative approaches are to approximate the correlation matrix with a Green's matrix (Karagiannidis et al., 2003) or assume exponential correlation (Aalo, 1995). We have chosen to use the latter, since it yields results that agree better with simulations.

4.3.1. Sparse sampling (case 2A) To find the PDF of the best out of $N_{\max}$ independent samples, we start by computing the CDF of a single sample. Hence, the PDF of the best sample is

$$f^{2\text{A}}_{\text{stop}}(\gamma) \triangleq \frac{\mathrm{d}}{\mathrm{d}z}\left[P(\gamma < z)^{N_{\max}}\right].$$

As above, the robot will spend a fraction $v_{\text{ref}}/v_{\max}$ driving at constant velocity, so the resulting PDF of the SNR will in this case be

$$f^{2\text{A}}_{\gamma}(\gamma) = \left(1 - \frac{v_{\text{ref}}}{v_{\max}}\right)f^{2\text{A}}_{\text{stop}}(\gamma) + \frac{v_{\text{ref}}}{v_{\max}}f^N_{\gamma}(\gamma). \quad (14)$$

This is illustrated in Figure 8, which assumes that $\delta = \lambda/2$, $\Delta_{\max} = \lambda$ and $v_{\text{ref}}/v_{\max} = 0.2$. We now turn to the case of correlated samples.

4.3.2. Dense sampling (case 2B) To compute the PDF for the best out of $N_{\max}$ correlated SNR samples, we use the approximation of exponential correlation as discussed above. The correlation coefficient of two adjacent SNR samples is $\rho = J_0^2(2\pi\delta/\lambda)$, where δ is the inter-sample distance. We then approximate the correlation between any two samples γ_j and γ_i as $\rho^{|j-i|}$. This allows us to compute the multivariate Nakagami CDF $P(\gamma_1 < z, \ldots, \gamma_{N_{\max}} < z)$ (Aalo, 1995). Similar to the above case, the resulting PDF is

$$f^{2\text{B}}_{\gamma}(\gamma) = \left(1 - \frac{v_{\text{ref}}}{v_{\max}}\right)f^{2\text{B}}_{\text{stop}}(\gamma) + \frac{v_{\text{ref}}}{v_{\max}}f^N_{\gamma}(\gamma), \quad (15)$$

where

$$f^{2\text{B}}_{\text{stop}}(\gamma) \triangleq \frac{\mathrm{d}}{\mathrm{d}z}P(\gamma_1 < z, \ldots, \gamma_{N_{\max}} < z).$$

It is illustrated in Figure 8, assuming $\delta = \lambda/12$, $\Delta_{\max} = \lambda$ and $v_{\text{ref}}/v_{\max} = 0.2$.

Comparing Figures 7 and 8, we see that both the partially informed stopping strategy and the fully informed stopping strategy succeed to improve the average SNR by moving the center of mass of the resulting PDFs, compared with the nominal Nakagami distribution. The staircase effect in the PDFs for the partially informed stopping strategy comes from the discrete thresholds, which are denser in case 1B than in case 1A, making the resulting PDF smoother. The quantitative differences between the cases will be clearer in the next section, where we use the resulting PDFs to compute expectations of the channel utilities.

5. Simulations

To illustrate the performance of the proposed strategies, we have compared simulations with the analytically computed expected utilities under various tracking constraints. We have also simulated a trajectory of the system under the partially informed stopping strategy, to clarify how it works. But first we describe the simulation setup.

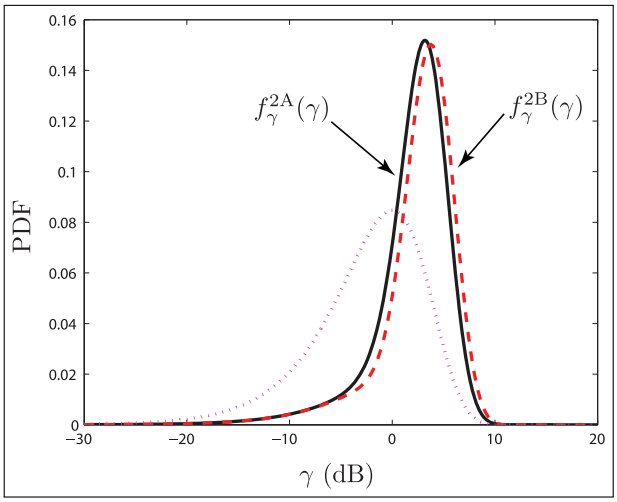

Fig. 8. An example of PDFs $f_\gamma^{2A}(\gamma)$ (case 2A) and $f_\gamma^{2B}(\gamma)$ (case 2B). 2A is the solid line and 2B is the dashed line. This shows the PDF of the resulting SNR when the robot has full knowledge of the SNR waveform, e.g. if this has been measured on a previous pass. The maximum tracking error is $\Delta_{\max} = \lambda$, so in case 2A, the robot always drives to the best of the 5 independent samples that it can reach, and in case 2B it has 30 correlated samples to choose from. The PDF for Nakagami fading (dotted line), is included for comparison. It corresponds to driving at constant velocity, as in case 0. Similar to Figure 7, communication-aware motion planning has shifted the centers of mass of the PDFs towards higher SNR than for the nominal case 0.

5.1. Simulation setup

In all simulations, we have assumed a distance of $\delta = \lambda/2$ between samples for sparse sampling and $\delta = \lambda/12$ for dense sampling. In the latter case, this yielded a correlation coefficient of $\rho = 0.87$ between adjacent samples. We also assumed Rayleigh fading ($m = 1$) and, unless specifically stated, an average SNR of $\Omega = 0$ dB. Further, we assumed that $v_{\text{ref}}/v_{\max} = 1/5$, so 20% of the time was spent driving. The bandwidth was chosen as $B = 1.15$ Hz so the capacity was normalized to 1 bit/s in case 0. We assumed QPSK modulation, with bit error probability $P_b(\gamma) = Q(\sqrt{\gamma})$ (Proakis and Salehi, 2002), where Q is the tail probability of the standard normal distribution. We further assumed a packet length of $M = 65$ bytes and normalized the throughput by assuming $R_0 = 1$ packet/s. Sparse sampling was simulated by generating independent samples from the distribution f_γ^N. To generate correlated samples, we used the Rayleigh fading simulator proposed by Zheng and Xiao (2003), setting the number of scatterers to 100.

5.2. Example trajectory

To illustrate the partially informed stopping strategy, we have simulated a trajectory of the system, with $\Delta_{\max} = \lambda$ and $\delta = \lambda/2$. We have chosen to maximize the capacity, i.e. $U = U_C$. Figure 9 shows the relative position, $\Delta(t)$ and the instantaneous SNR, $\gamma(t)$ during 8 s of the trajectory. The robot stops when it finds a high SNR value, creating long periods of high capacity. This reshapes the resulting SNR distribution towards higher SNR, compared with the Nakagami distribution. When the robot stands still, $\Delta(t)$ decreases. The SNR is constant, but the stop threshold $\bar{\gamma}(N)$ increases as the number, N, of reachable samples in front of the robot increases. Eventually the robot starts driving again, either because the SNR is below the threshold or if $\Delta(t) = -\Delta_{\max}$. Similarly, the robot will always stop before driving past $\Delta(t) = \Delta_{\max}$ since $\bar{\gamma}(N = 0) = 0$.

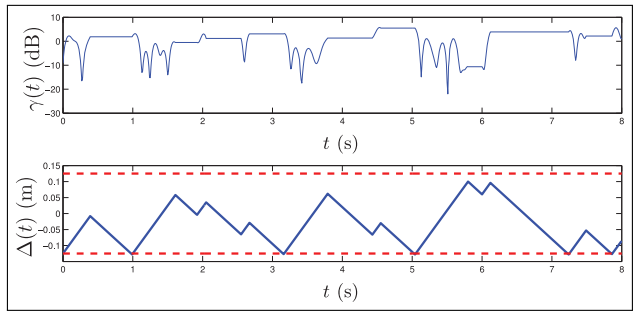

Fig. 9. An example trajectory when using the partially informed stopping strategy. When the robot drives, the SNR, γ, varies. By stopping at positions where γ is high, it can increase the average link capacity. The relative position, $\Delta(t)$, increases when the robot drives, and decreases when it stands still. The robot samples $\gamma(x_i)$ and stops if it exceeds the stop threshold. The dashed lines depict $\pm\Delta_{\max}$, which are the tracking error bounds.

5.3. Utility versus tracking tolerance

To illustrate how the expected utility, $U(\gamma)$, improves when the tracking tolerance, $\Delta_{\max}$, is increased, we have used the PDFs (2), (11), (13), (14), and (15) to compute the expectation. We have also compared with simulations, for each of the five cases. The results, both for capacity, $U = U_C$, and throughput, $U = U_T$, show that the greatest gain in utility is achieved already when allowing small deviations from the reference. Table 2 shows $N_{\max}$, i.e. the maximal number of reachable samples for the robot, for each value of $\Delta_{\max}$.

Figure 10 shows the resulting expected capacity, U_C, in all five cases. As expected, knowledge of the full waveform yields higher expected capacity than just knowing the nominal SNR distribution. This is true both for sparse sampling (cases 1A and 2A) and dense sampling (cases 1B and 2B). Also, dense sampling provides more information than sparse sampling, which results in higher capacity. The differences between simulation and theory for cases 1B and 2B come from the approximations described above, used to handle the correlation between non-adjacent samples. We finally note that for wireless communication at 2.4 GHz, allowing a tracking error in the order of 0.5 m (4λ) can offer a doubling of the link capacity, even with knowledge only of the nominal fading distribution.

Figure 11 shows analytical predictions and simulation results of how the expected throughput, U_T, varies with

Table 2. Maximal number of reachable samples, $N_{\max}$.

$\Delta_{\max}$	$\lambda/4$	$\lambda/2$	λ	$3\lambda/2$	2λ	3λ	4λ
Independent	1	2	5	7	10	15	20
Correlated	7	15	30	45	60	90	120

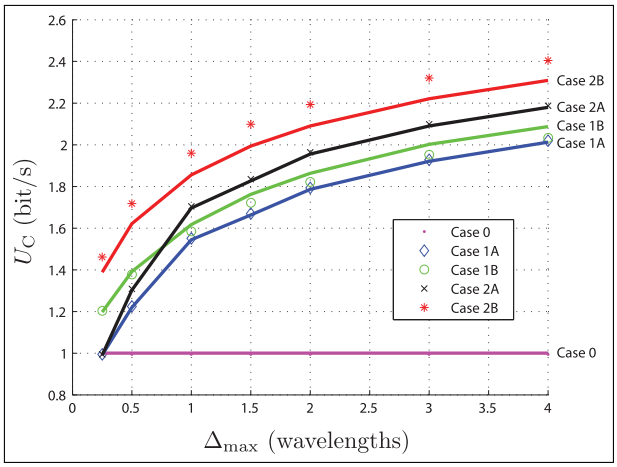

Fig. 10. Expected link capacity, U_C, as a function of the tracking error tolerance, $\Delta_{\max}$, for the five cases considered. The bandwidth B was chosen so the capacity is 1 in the nominal case 0. The capacity increases fastest for small $\Delta_{\max}$. Analytical predictions are drawn as solid lines, labeled on the right, and simulations are shown as markers.

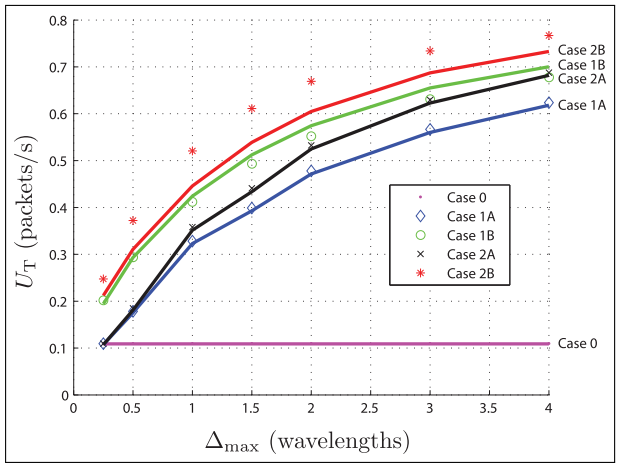

Fig. 11. Expected link throughput, U_T, as a function of the tracking error tolerance $\Delta_{\max}$, for the five cases considered. The maximum throughput was chosen as $R_0 = 1$ packet/s for normalization. The throughput increases most rapidly for small $\Delta_{\max}$. Analytical predictions are drawn as solid lines, labeled on the right, and simulations are shown as markers.

the tracking error tolerance, $\Delta_{\max}$. Here we have assumed a mean SNR of $\Omega = 3$ dB, which yields a throughput of 0.11 packets/s. Similar to the case of capacity, the throughput increases most rapidly for small tracking error tolerances. Both the analytical prediction and the simulations show that case 1B yields higher throughput than case 2A. This means that full knowledge of the SNR is less important than sampling densely when optimizing for throughput. A possible explanation is that $U_T(\gamma)$ transitions from 0 to R_0 in a very narrow SNR interval. Thus, exploring and stopping at the first SNR sample with reasonable throughput yields similar performance as finding the highest SNR inside the tracking window. As above, we note that for a 2.4 GHz link with low nominal throughput, allowing a tracking error of 0.5 m (4λ) can yield a throughput improvement of five times or more.

6. Experimental evaluation

The first objective of our experiments was to validate the model of static Nakagami fading by measurements in various environments. The second objective was to implement the proposed method and compare it with the nominal case 0. We have tested this in environments that exhibit static fading, as well as where the fading is more time-varying, to investigate the robustness of the approach. Before going into the experiment results, we describe the setup.

6.1. Experiment setup

We used an indoor differential drive robot, equipped with a laptop and two Tmote Sky transceivers. The Tmote Sky is an IEEE 802.15.4 compliant transceiver operating at 2.4 GHz, using QPSK modulation with a data rate of 250 kbit/s, output power of 0 dBm and an internal antenna with approximately omnidirectional radiation pattern (Moteiv Corporation, 2006). As illustrated in Figure 12, one transceiver was used for measurements. It listened to another Tmote Sky which acted as base station, broadcasting $R_0 = 64$ packets/s, each $M = 65$ bytes long. The other transceiver, using another channel, received steering commands for the robot from an operator, acting as a path planner. Letting the robot autonomously control its forward velocity while manually steering it along the path, allowed quick setup at various test locations, without the need for any navigation other than odometry. The paths were chosen so different segments were never closer than $\lambda/2$, to avoid undesired correlation between measurements. The robot measured the RSS, which in logarithmic scale is related to the SNR by a constant offset. Measurements of the background noise levels in the various locations indicate a constant noise level of -96 dBm in the Tmote Sky, with a standard deviation of about 1 dB.

The experiments were carried out in six locations on the KTH campus, chosen to represent various degrees of

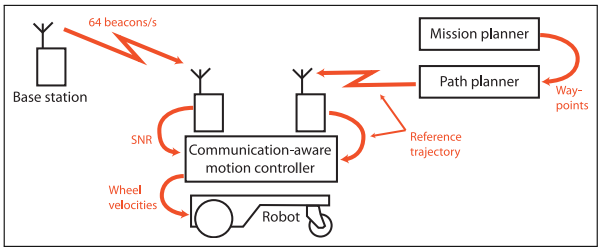

Fig. 12. Experiment setup. A communication-aware motion controller onboard the robot computes the wheel velocities based on the reference trajectory and the SNR of the beacons from the base station. The reference trajectory in transmitted from a path planner, which finds obstacle-free trajectories between waypoints specified by a mission planner.

motion in the environment. The sites are listed in Table 3, where the level of activity at each site is judged on a scale of 0 (empty), 1 (people passing now and then) and 2 (crowded). Figure 13 contains photos of each site, to illustrate the type of environment and the activity level. Below, we describe how the model validation measurements were performed at each site.

6.2. Model validation

To investigate the applicability of the communication model of static Nakagami fading, we have compared the distribution of the RSS while driving to the distribution when standing still, at each experiment site.

In the experiments, we measured the RSS while driving along a path. To isolate the multipath fading from the effects of path loss and shadowing, we subtracted the moving average of the RSS, computed over a window of 1 m. This length was empirically chosen so the path loss and shadowing would be approximately constant inside the window. We then estimated the Nakagami parameter m as in (3) for the deviations from the moving average and compared the resulting CDF, $F^N(\gamma)$, with the empirical distribution function, $F(\gamma)$, of our observations. As a metric of the goodness of fit, we have used the Kolmogorov–Smirnov (K–S) statistic (Massey, 1951)

$$D \triangleq \sup_{\gamma} |F^N(\gamma) - F(\gamma)|.$$

Then we measured the RSS while the robot was standing still at five positions along the path, 2 min at each. For each set of measurements, we estimated m for the deviations from the mean. We also estimated m_{tot}, which we define as the Nakagami m-parameter for the total SNR histogram of all five stops. Note that the deviations have a mean of about 0 dB, so m is inversely proportional to the SNR variance. High values of m correspond to a narrow distribution, which means that the assumption on static fading is valid.

Site 1 was a workshop, full of machinery and metal cabinets, but with no people present. The results of driving in site 1 are shown in Figure 14. On the left are the RSS samples taken when driving, with the moving average superimposed as a thick line. On the right is the normalized RSS histogram with the best-fit Nakagami PDF $f_\gamma^N(\gamma)$ (solid line) superimposed, with $m = 1.53$. The K–S statistic was $D = 0.048$.

The RSS recorded when standing still at site 1 is depicted in Figure 15. Each subfigure corresponds to a stop of 2 min at some position along the path. The Nakagami parameters, m, are 180, 27, 64, 77 and 240. At this site, $m_{\text{tot}} = 91$. This was the most static of our measurement locations and the values of m are almost two orders of magnitude higher than those when driving, which indicates that the assumption of static fading is very accurate in this environment.

The most crowded location was site 6, a busy hallway during daytime, with students walking past the robot during the experiment. The results when driving are shown in Figure 16 and m was estimated to 1.77. The RSS measured when standing still is shown in Figure 17 and m was 17, 19, 19, 8.3 and 13. The values of m are one order of magnitude less than those in the workshop, which makes this the least static of our locations. Nevertheless, even at this location, the RSS variance is about one order of magnitude less when standing still than when driving. In the next subsection, we will see how this affects the resulting channel quality improvement.

Table 3 summarizes the results of all validation experiments, with the sites ordered by decreasing m_{tot}. The table suggests that the estimated Nakagami parameter m_{tot} is useful for reflecting the activity level. The results show that the estimated Nakagami m parameter for the RSS distribution ranges from 1.4 to 1.9, which indicates that the fading is slightly less severe than Rayleigh fading. Each RSS histogram contained about 23 000 samples, so the theoretical limit for the K–S test at 1% risk of false rejection is $D = 0.01$ (Massey, 1951). Despite measurement noise and occasional packet losses, the measured values of D are well within the same order of magnitude, which indicates that the Nakagami distribution is a meaningful model in this environment. With regards to the assumption on static fading, all sites exhibited values of m that were one or two orders of magnitude larger when standing still than when driving. This indicates that even if the fading is not perfectly static, it makes sense to stop to communicate if the RSS is high. The assumption on static fading is thus motivated in all locations tested. In the next section, we will see how the degree of static fading affects the resulting channel utility when implementing the partially informed stopping strategy.

6.3. Results

As a proof of concept and to investigate what happens when the fading is less static, we have implemented the proposed method and tested it experimentally at all six sites. The results of all experiments are listed in Table 4, numbered so that experiments 1A–1D were performed at site 1 and

Fig. 13. The experiment sites for model validation and comparison of the proposed strategies, numbered from left to right, top row first. Sites 1–3 were empty, sites 4 and 5 had people passing now and then and site 6 was crowded.

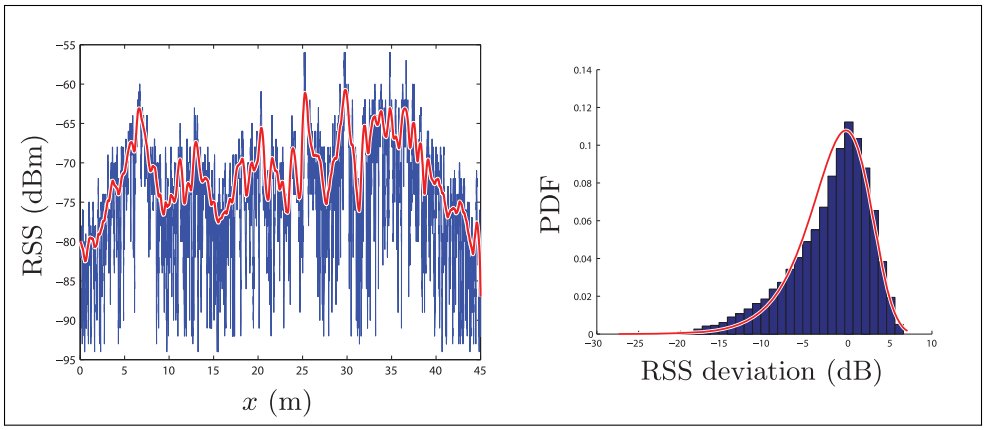

Fig. 14. Measurements of the RSS when driving at constant velocity in site 1, a cluttered but unattended workshop. The left graph shows the RSS and the moving average (thick line). The right graph shows the normalized histogram of the deviations from the moving average and the corresponding best-fit Nakagami PDF (solid line), with $m = 1.53$.

Table 3. Measured fading parameters.

Site	Description (Activity level)	Driving		Standing still					m_{tot}
		m	D			m			
1	Workshop (0)	1.53	0.048	180	27	64	77	240	91
2	Corridor (0)	1.92	0.031	100	80	41	18	62	78
3	Storage (0)	1.60	0.021	58	36	360	125	99	75
4	Lab (1)	1.38	0.024	49	17	27	28	22	23
5	Corridor (1)	1.54	0.030	14	27	68	42	5.2	14
6	Hallway (2)	1.77	0.032	17	19	19	8.3	13	13

so on. The method was tested using the partially informed stopping strategy for independent samples (case 1A). As a comparison, we have used the uninformed stopping strategy (case 0). We have allowed a maximum tracking error of $\Delta_{\max} = 2\lambda = 25$ cm and a sample spacing of $\delta = \lambda/4 = 3.1$ cm. The velocities were $v_{\text{ref}} = 2.5$ cm/s and $v_{\max} = 12.5$ cm/s. To adapt the stop thresholds to changes in path loss and shadowing along the path, we have continuously estimated the nominal RSS distribution based on previous measurements. To avoid biasing the estimate, we have only used measurements taken when driving.

Figure 18 shows an example trajectory of the system, during experiment 6A in the crowded corridor. The upper graph shows the RSS (dots) of each received packet. If the

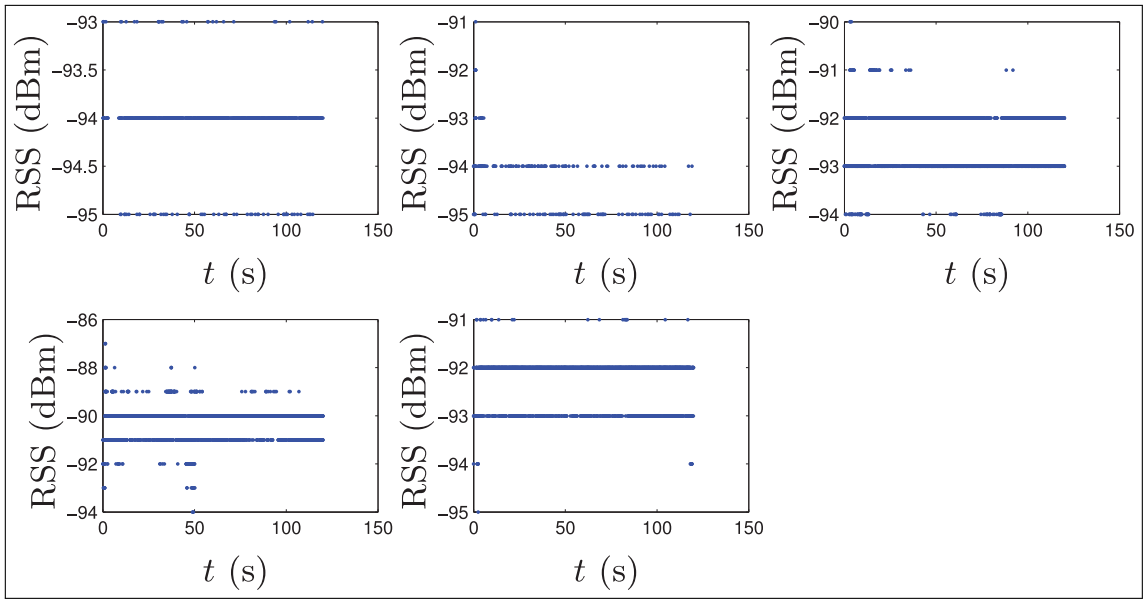

Fig. 15. Measurements of the RSS when standing still at five different locations along the path at site 1. The Nakagami parameter m for each measurement set is 180, 27, 64, 77 and 240, starting with the top row. High values of m correspond to a narrow RSS distribution, which indicates that this location exhibits almost static fading.

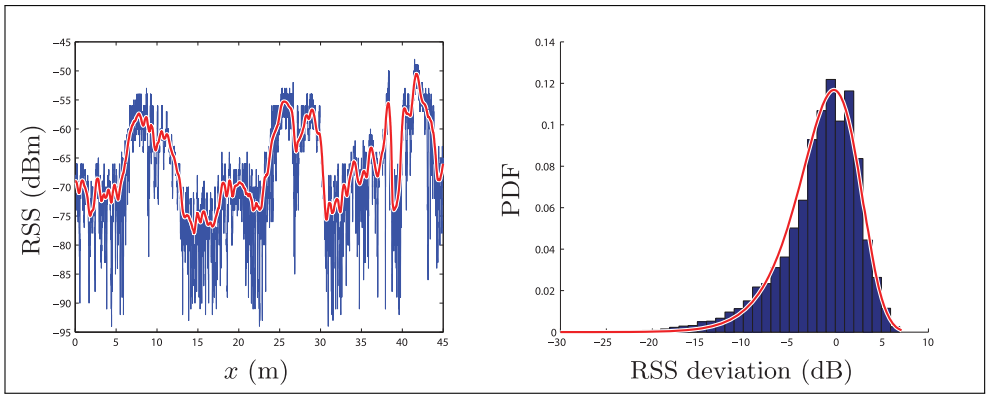

Fig. 16. Measurements of the RSS when driving at constant velocity at site 6, a crowded corridor. The left graph shows the RSS and the moving average (thick line). The right graph shows the normalized histogram of the deviations from the moving average and the corresponding best-fit Nakagami PDF (solid line), with $m = 1.77$.

robot reaches a sampling point x_j and the RSS is higher than the stop threshold, it stops. As $\Delta(t)$ decreases during the stop, the RSS will be compared with increasingly higher thresholds, as defined in the partially informed stopping strategy, until the robot starts driving again. The RSS level corresponding to the lowest threshold (solid line), $\bar{\gamma}(1)$, is included in the graph for illustration. Note how the threshold changes as the estimate of the nominal RSS distribution is updated. Also note the complete outage for 25 s at $t = 325$ s. Owing to shadowing, almost all packets are lost in this interval, so the robot follows the forward edge of the tracking window until the outage stops. This happened very frequently in all tests, reducing the efficiency of the proposed strategy. We believe that these variations due to shadowing are the main reason for the differences between the measured throughput and the analytical prediction, which assumes constant mean SNR, Ω, during the whole experiment. The shadowing also causes stronger correlation between SNR samples than predicted by the analysis. This means that the robot would need to make larger deviations from the reference position to efficiently exploit the SNR variations. This is a possible direction of future research, as discussed in Section 7.

Table 4 summarizes the results of all experiments. For each test, it shows the number, the location and the average throughput when following the uninformed stopping strategy (case 0) and when following the partially informed stopping strategy (case 1A). The maximum throughput is 64 packets/s. Finally, the table also states the throughput improvement for each test.

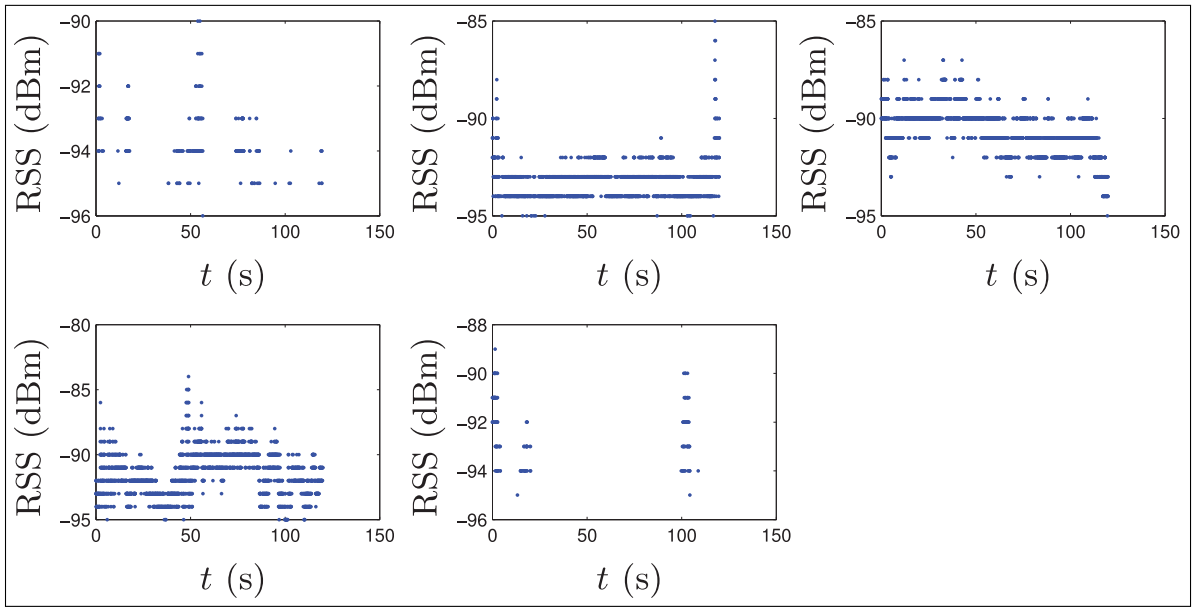

Fig. 17. Measurements of the RSS when standing still at five different locations along the path at site 6. The Nakagami parameter m is 17, 19, 19, 8.3 and 13, starting with the top row. This shows that this location exhibits less static fading than the workshop. The sparsity of the first and last graph comes from frequent packet losses.

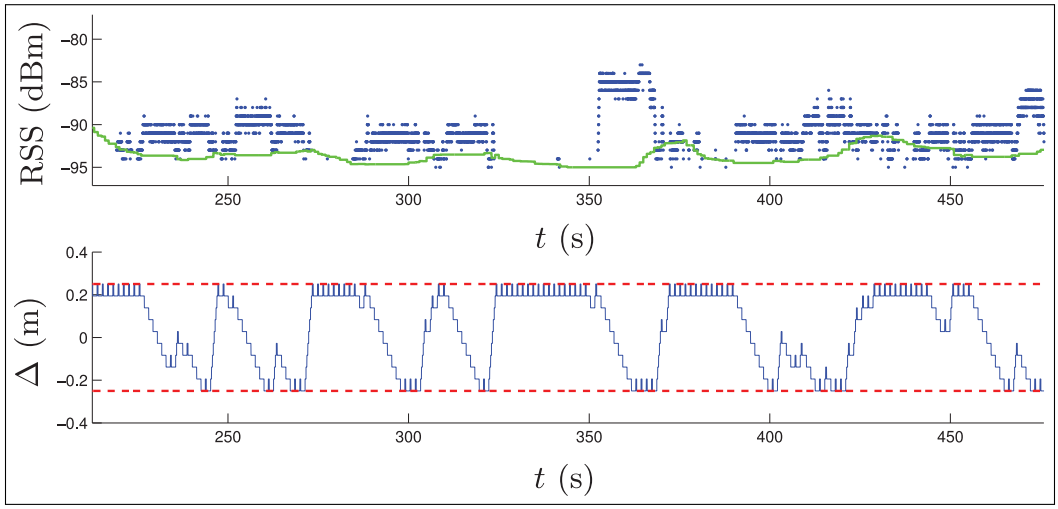

Fig. 18. Partial system trajectory during test 6A in the crowded corridor. The dots in the upper graph denote the RSS of received packets and the solid line is the lowest stop threshold, corresponding to $\bar{\gamma}(1)$. If the RSS at a sampling point, x_j, is higher than the threshold, the robot stops. Stopping causes periods of high RSS, which increases the average throughput, compared with driving at constant velocity. The lower graph shows the relative position, Δ, which is constrained to $\pm\Delta_{\max}$, shown by the dotted lines.

To interpret the results, Figure 19 shows the throughput improvement of each experiment, plotted against the nominal throughput of case 0. For comparison, we have included the analytic prediction, computed using (11), $m = 1.5$ and Ω chosen so that the expected throughput for case 0 equals the measured throughput. As commented above, this represents an ideal case, when Ω is constant, so there is no change in the path loss or shadowing. Figure 19 shows that the approach is robust to moderate violations of the assumption of static fading, in the sense that there is no clear difference between the results from empty sites and sites with moderate motion. Site 6, however, clearly shows lower throughput improvements than the trend of the other experiments. The figure also illustrates that stop-and-go motion yields the highest throughput improvements, over 100%, in regions where the nominal throughput is low. If the nominal channel quality is high, stop-and-go motion is less motivated.

7. Conclusions

Given a reference trajectory and an associated tracking tolerance, $\Delta_{\max}$, we have proposed and analyzed two novel

Table 4. Experiment results.

Experiment no.	Description (activity level)	U_T (packets/s)		Improvement
		Case 0	Case 1A	
1A	Workshop (0)	12	28	130%
1B		11	23	120%
1C		49	57	18%
1D		48	56	16%
2A	Corridor (0)	42	53	27%
2B		35	47	33%
3A	Storage (0)	36	51	44%
3B		46	57	25%
3C		23	39	68%
3D		6.3	13	110%
4A	Lab (1)	5.3	15	190%
4B		21	37	76%
4C		22	36	68%
4D		44	53	20%
5A	Corridor (1)	26	44	68%
5B		10	22	120%
5C		6.3	16	150%
5D		4.4	14	230%
6A	Hallway (2)	28	36	28%
6B		20	27	40%

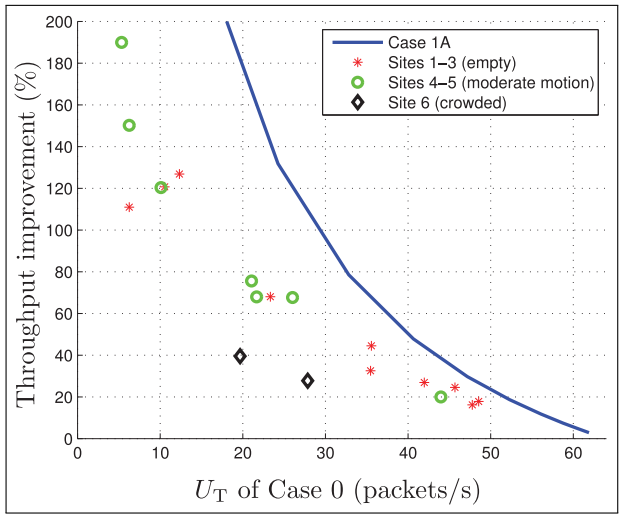

Fig. 19. Throughput improvement of the experiments, as a function of the nominal throughput of case 0. The experiment results are categorized according to the judged activity level. The results show that the partially informed stopping strategy can yield significant throughput improvements if the nominal link utility is low. Also, the strategy is robust to moderate levels of motion in the environment.

strategies for communication-aware motion planning: if the SNR, $\gamma(x_i)$, is fully known, the robot should spend as much time as possible at the position with highest SNR inside the tracking window. If the nominal SNR distribution is known (or can be estimated), the robot can use an optimal stopping exploration approach to spend time at positions that maximize the expected channel utility.

The analysis shows that the expected link capacity or throughput can be significantly increased even by allowing small tracking errors, of the order of 2–4 wavelengths. Increasing the tracking tolerance above this yields less improvements. Having full knowledge of the SNR, as in cases 2A and 2B, offers some performance improvements, at the price of high requirements on the navigation accuracy and the need to acquire the SNR information beforehand. Owing to this, it is primarily treated as a benchmark case. For both cases 1A/1B and 2A/2B, increasing the sampling density provides a marginal increase in performance, at the price of significantly higher complexity in the analysis and (for case 1B) computing the stop thresholds. This is analogous to the analysis of uniform linear antenna arrays, where is can be shown that the spectral efficiency quickly converges as the number of antenna elements in a given space increase (Muharemovic et al., 2008). As shown in Figure 19, the proposed strategies are most motivated in the region where the link quality is low.

Our measurements in various locations validated the model of static Nakagami fading. The SNR variance was one or two orders of magnitude less when standing still than when driving, which motivates stopping at positions with high SNR to improve the average utility over time. Experiments showed that the proposed partially informed stopping strategy is robust to moderate levels of motion in the environment and that it can consistently deliver throughput improvements of over 100% when the channel quality is low.

This paper focuses on the channel between a single robot and its base station. But similar principles are applicable in multi-robot networks, where robots also communicate between each other. A simple extension is when robots are deployed to static locations and the communication topology is a tree. Starting from the root, the robots could then sequentially make small movements to improve the channel to their parent with respect to multipath fading. For other topologies, one could use a distributed optimization framework (Vieira et al., 2011). If two moving robots are communicating, they could jointly decide to stop when the channel is good. In a static environment, this is equivalent to the case of a base station and a single robot. And if both robots have the same reference velocity, the tradeoff between communication and reference tracking is identical, so they can make the same stopping decisions.

There are many other approaches for exploiting multipath fading, such as multi-antenna diversity, frequency diversity, polarization and time diversity (Molisch, 2005). These methods can improve the SNR of a single link, but in a dense network, the total throughput is instead limited by interference (Gupta and Kumar, 2000). In such settings, multiuser diversity has been shown to improve the network-wide performance. Mobile nodes can use mobility to relay delay-tolerant messages and reduce the impact of

interference (Grossglauser and Tse, 2002). In a multipath fading environment, nodes may instead use opportunistic communication, i.e. communicating with the neighbor to which they have the best channel at the moment (Viswanath et al., 2002). The proposed stop-and-go motion could be described as a type of antenna diversity, reusing a single moving antenna instead of an antenna array. As mentioned above, cases 2A and 2B correspond to selection combining, where a receiver uses the antenna with the best SNR. There are also parallels between the optimal stopping in cases 1A and 1B and switch-and-examine diversity (Alexandropoulos et al., 2010). This paper aims at providing a complement to already existing diversity techniques. Stop-and-go motion can provide an alternative to antenna diversity for very small robots, where multiple antennas cannot be mounted with enough separation. Also, it does not require any extra hardware, but instead leverages the mobility of the robot. The proposed methods can also be used in combination with other diversity types, for improved performance. As an example, for a robot with three antennas or three alternative frequencies, also choosing between three independent sampling positions provides nine independent channels and thus higher diversity gain than each separate method.

During the experiments, we observed that shadowing caused periods of complete outage, when the proposed strategies were ineffective. Since the analysis assumes constant path loss and shadowing, this appears to be the main reason why the experiments only reached about 60% of the predicted throughput improvements. For future work, it would be interesting to increase the tracking tolerance to the spatial scale of the shadowing, to allow the robot to quickly pass areas with unfavorable shadowing. Another interesting extension would be to use transmitters with higher output power, such as mobile phone base stations, which would allow the robot to operate farther from the base station. This can be expected to lead to more constant path loss and shadowing, which would be beneficial for the performance of the proposed strategies.

Funding

This work was supported by the Swedish Defence Materiel Administration through the TAIS project; the European Commission through the RUNES and HYCON projects; the Swedish Research Council; and the Swedish Foundation for Strategic Research.

References

Aalo VA (1995) Performance of maximal-ratio diversity systems in a correlated Nakagami-fading environment. *IEEE Transactions on Communications* 43(8): 2360–2369.

Alexandropoulos GC, Mathiopoulos PT and Sagias NC (2010) Switch-and-examine diversity over arbitrarily correlated Nakagami-m fading channels. *IEEE Transactions on Vehicular Technology* 59(4): 2080–2087.

Anisi D, Ögren P and Hu X (2010) Cooperative minimum time surveillance with multiple ground vehicles. *IEEE Transactions on Automatic Control* 55(12): 2679–2691.

Babich F and Lombardi G (2000) Statistical analysis and characterization of the indoor propagation channel. *IEEE Transactions on Communications* 48(3): 455–464.

Chow YS (1971) *Great expectations: The theory of optimal stopping*. Houghton Mifflin.

Chung TH, Burdick JW and Murray RM (2006) A decentralized motion coordination strategy for dynamic target tracking. In: *Proceedings of the IEEE International Conference on Robotics and Automation*, Orlando, FL.

Dixon C and Frew EW (2009) Maintaining optimal communication chains in robotic sensor networks using mobility control. *Mobile Networks and Applications* 14(3): 281–291.

Esposito JM and Dunbar TW (2006) Maintaining wireless connectivity constraints for swarms in the presence of obstacles. In: *Proceedings of the IEEE International Conference on Robotics and Automation*, Orlando, FL.

Ganguli A, Cortés J and Bullo F (2009) Multirobot rendezvous with visibility sensors in nonconvex environments. *IEEE Transactions on Robotics* 25(2): 340–352.

Ghaffarkhah A and Mostofi Y (2011) Communication-aware motion planning in mobile networks. *IEEE Transactions on Automatic Control* 56(10): 2478–2485.

Grossglauser M and Tse DNC (2002) Mobility increases the capacity of *ad hoc* wireless networks. *IEEE/ACM Transactions on networking* 10(4): 477–486.

Gupta P and Kumar PR (2000) The capacity of wireless networks. *IEEE Transactions on Information Theory* 46(2): 388–404.

Hollinger G and Singh S (2010) Multi-robot coordination with periodic connectivity. In: *Proceedings of the IEEE International Conference on Robotics and Automation*, Anchorage, AK.

Hsieh MA, Cowley A, Kumar RV and Taylor CJ (2008) Maintaining network connectivity and performance in robot teams. *Journal of Field Robotics* 25(1–2): 111–131.

Jakes WC (ed.) (1974) *Microwave Mobile Communications*. IEEE Press.

Ji M and Egerstedt M (2007) Distributed coordination control of multiagent systems while preserving connectedness. *IEEE Transactions on Robotics* 23(4): 693–703.

Karagiannidis GK, Zogas DA and Kotsopoulos SA (2003) An efficient approach to multivariate Nakagami-m distribution using Green's matrix approximation. *IEEE Transactions on Wireless Communications* 2(5): 883–889.

Lindhé M and Johansson KH (2009) Using robot mobility to exploit multipath fading. *IEEE Wireless Communications* 16(1): 30–37.

Lindhé M, Johansson KH and Bicchi A (2007) An experimental study of exploiting multipath fading for robot communications. In: *Proceedings of Robotics: Science and Systems*, Atlanta, GA.

Lindhé M, Keviczky T and Johansson KH (2011) Multi-robot path following with visual connectivity. In: *Proceedings of the Asilomar Conference on Signals, Systems and Computers*, Pacific Grove, CA.

Massey FJ (1951) The Kolmogorov–Smirnov test for goodness of fit. *Journal of the American Statistical Association* 46(253): 68–78.

Molisch AF (2005) *Wireless Communications*. New York: John Wiley and Sons Ltd.

Moser L (1956) On a problem of Cayley. *Scripta Mathematica* 22: 289–292.

Mostofi Y (2009) Decentralized communication-aware motion planning in mobile networks: an information-gain approach. *Journal of Intelligent and Robotic Systems* 56(2): 233–256.

Moteiv Corporation (2006) Tmote Sky datasheet 1.02. http://www.moteiv.com (accessed 19 May 2007).

Muharemovic T, Sabharwal A and Aazhang B (2008) Antenna packing in low-power systems: Communication limits and array design. *IEEE Transactions on Information Theory* 54(1): 429–440.

Proakis JG and Salehi M (2002) *Communication Systems Engineering*, 2nd edn. Prentice-Hall.

Puccinelli D, Brennan M and Haenggi M (2007) Reactive sink mobility in wireless sensor networks. In: *First ACM Workshop on Mobile Opportunistic Networking*, Puerto Rico.

Puccinelli D and Haenggi M (2006) Multipath fading in wireless sensor networks: Measurements and interpretation. In: *Proceedings of the International Wireless Communications and Mobile Computing Conference*.

Rubio L, Reig J and Cardona N (2007) Evaluation of Nakagami fading behaviour based on measurements in urban scenarios. *AEU International Journal of Electronics and Communications* 61(2): 135–138.

Sarkar TK, Ji Z, Kim K, Medouri A and Salazar-Palma M (2003) A survey of various propagation models for mobile communication. *IEEE Antennas and Propagation Magazine* 45(3): 51–82.

Sheikh A, Abdi M and Handforth M (1993) Indoor mobile radio channel at 946 MHz: Measurements and modeling. In: *Proceedings of the 43rd IEEE Vehicular Technology Conference*, Secaucus, NJ.

Simon MK and Alouini MS (1998) A simple integral representation of the bivariate Rayleigh distribution. *IEEE Communications letters* 2(5): 128–130.

Smith J, Olivieri M, Lackpour A and Hinnerschitz N (2009) RF-mobility gain: concept, measurement campaign, and exploitation. *IEEE Wireless Communications* 16(1): 38–44.

Spanos DP and Murray RM (2004) Robust connectivity of networked vehicles. In: *Proceedings of the IEEE International Conference on Robotics and Automation*, New Orleans, LA.

Stachura M and Frew EW (2011) Cooperative target localization with a communication-aware unmanned aircraft system. *AIAA Journal of Guidance, Control, and Dynamics* 34(5): 1352–1362.

Stüber GL (1996) *Principles of mobile communication*. Dordrecht: Kluwer Academic Publishers.

Stump E, Jadbabaie A and Kumar V (2008) Connectivity management in mobile robot teams. In: *Proceedings of the IEEE International Conference on Robotics and Automation*, Pasadena, CA.

Sweeney J, Grupen R and Shenoy P (2004) Active QoS flow maintenance in controlled mobile networks. In: *Proceedings of the Fourth International Symposium on Robotics and Automation*, Queretaro, Mexico.

Tekdas O, Plonski PA, Karnad N and Isler V (2010) Maintaining connectivity in environments with obstacles. In: *Proceedings of the IEEE International Conference on Robotics and Automation*, Anchorage, AK.

Varaiya P (2000) A question about hierarchical systems. In: Djaferis T and Schick I (eds.) *System Theory: Modeling, Analysis and Control*. Dordrecht: Kluwer.

Vieira MAM, Taylor ME, Tandon P, et al. (2011) Mitigating multipath fading in a mobile mesh network. *Ad Hoc Networks*. DOI: 10.1016/j.adhoc.2011.01.

Viswanath P, Tse DNC and Laroia R (2002) Opportunistic beamforming using dumb antennas. *IEEE Transactions on Information Theory* 48(6): 1277–1294.

Zavlanos MM, Tanner HG, Jadbabaie A and Pappas GJ (2009) Hybrid control for connectivity preserving flocking. *IEEE Transactions on Automatic Control* 54(12): 2869–2875.

Zhang QT and Lu HG (2002) A general analytical approach to multi-branch selection combining over various spatially correlated fading channels. *IEEE Transactions on Communications* 50(7): 1066–1073.

Zheng YR and Xiao C (2003) Simulation models with correct statistical properties for Rayleigh fading channels. *IEEE Transactions on Communications* 51(6): 920–928.